Comput Mech (2010) 46:363–375
DOI 10.1007/s00466-010-0479-z

ORIGINAL PAPER

A finite strain framework for the simulation of polymer curing. Part II. Viscoelasticity and shrinkage

M. Hossain · G. Possart · P. Steinmann

Received: 13 August 2009 / Accepted: 29 January 2010 / Published online: 17 February 2010

Abstract A phenomenologically inspired, *elastic* finite strain framework to simulate the curing of polymers has been developed and discussed in the first part (Hossain et al. in Comput Mech 44(5):621–630, 2009) of this work. The present contribution provides an extension of the previous simulation concept towards the consideration of *viscoelastic* effects and the phenomenon of *curing shrinkage*. The proposed approach is particularly independent of the type of the free energy density, i.e. any phenomenologically or micromechanically based viscoelastic polymer model can be utilised. For both cases the same representatives that have been used for the elastic curing models, i.e. the Neo-Hookean model and the 21-chain microsphere model, are reviewed and extended accordingly. The governing equations are derived as well as the corresponding tangent operators necessary for the numerical implementation within the finite element method. Furthermore, we investigate two different approaches—a shrinkage strain function and a multiplicative decomposition of the deformation gradient–to capture the phenomenon of curing shrinkage, i.e. the volume reduction induced by the polymerisation reaction which may lead to significant residual stresses and strains in the fully cured material. Some representative numerical examples conclude this work and prove the capability of our approach to correctly capture inelastic behaviour and shrinkage effects in polymers undergoing curing processes.

M. Hossain · G. Possart · P. Steinmann (✉)
Chair of Applied Mechanics, University of Erlangen-Nuremberg,
Egerlandstrasse 5, 91058 Erlangen, Germany
e-mail: paul.steinmann@ltm.uni-erlangen.de

M. Hossain
e-mail: mokarram.hossain@ltm.uni-erlangen.de

G. Possart
e-mail: gunnar.possart@ltm.uni-erlangen.de

Keywords Polymers · Curing · Finite strains · Viscoelasticity · Shrinkage

1 Introduction and outline

The increasing application of reactive polymer systems like epoxy- or PU-adhesives in automotive, electronics or aerospace industry necessitates the development of simulation concepts and constitutive models that consider the time-dependence exhibited by relevant mechanical properties like the elastic stiffness, viscosity or relaxation time. Uncured polymer solutions usually behave as deformable viscous liquids mainly incapable of sustaining any load other than hydrostatic. During the curing process, polymer chains emerge from the constituents of the solution, possibly crosslink to each other and stiffness, viscosity and molecular weight increase. To especially account for the temporal evolution of inelastic material properties is not only necessary until the material has passed its gel point, but also due to the fact that almost every cured polymer possesses rate dependent creep and relaxation effects. Both are highly dependent on the particular structure and observable as rather fast processes with relaxation times in the order of seconds, e.g. for elastomers, as well as very slow ones taking several days like in epoxies.

Concerning previous contributions on modelling and simulation of curing phenomena in polymers we refer to the literature cited in the prequels [1] and [2] of this work. Real-world applications of the simulation concept proposed subsequently would be reliant on experimental data for the evolution of material parameters during the curing process, e.g. on time-dependent values for stiffness, viscosity and/or relaxation time. The number of publications concerning this

matter is unfortunately still rather limited, some references have been given in [2].

The foundation of all viscoelastic curing models proposed in the following is provided by the hypoelastic constitutive equation

$$\dot{\boldsymbol{S}}(t) = \mathbb{C}(t) : \dot{\boldsymbol{E}}(t) = \frac{1}{2}\mathbb{C}(t) : \dot{\boldsymbol{C}}(t), \tag{1}$$

relating the material time derivative of the second Piola–Kirchhoff stress tensor $\boldsymbol{S}$ to that of the Green–Lagrange strain $\boldsymbol{E} = \frac{1}{2}[\boldsymbol{C} - \boldsymbol{I}]$, itself depending on the right Cauchy–Green strain tensor $\boldsymbol{C} = \boldsymbol{F}^t \cdot \boldsymbol{F}$, via a *time-dependent* fourth-order *stiffness operator* $\mathbb{C}(t)$. The particular format of this equation has been phenomenologically motivated in [2], its appropriateness to reproduce the behaviour of *elastically* curing materials was demonstrated in [1]. The stiffness operator $\mathbb{C}(t)$ required in (1) is computed according to

$$\mathbb{C}(t) = 4\frac{\partial^2 \Phi(t)}{\partial \boldsymbol{C}^2} \tag{2}$$

from an arbitrary free energy density Φ, which in turn has to be chosen adequately with respect to the material under consideration. Note that both Φ and the corresponding stiffness $\mathbb{C}$ are not only implicitly time dependent via the loading history $\boldsymbol{C}$, but also explicitly due to the temporal evolution experienced by the governing material parameters during the curing process.

Constitutive ansatz (1) ensures by design that the stress state changes if and only if the strain state $\boldsymbol{C}$ is modified—although especially the stiffness of the material is increasing permanently in consequence of the polymer network formation. As for any other constitutive assumption, the question for thermodynamical consistency arises in view of Eq. (1). This issue was addressed in detail within [1], where we have demonstrated that an *accumulated energy density* Ψ, implicitly dependent on $\Phi(t)$ via the stiffness $\mathbb{C}(t)$ and defined by the convolution integral

$$\Psi(t) = \frac{1}{2}\int_0^t \left[\mathbb{C}'(s) : [\boldsymbol{E}(t) - \boldsymbol{E}(s)]\right] : [\boldsymbol{E}(t) - \boldsymbol{E}(s)]ds, \tag{3}$$

provides, according to the standard Coleman–Noll argumentation on the isothermal dissipation inequality

$$\boldsymbol{S} : \dot{\boldsymbol{E}} - \dot{\Psi} \geq 0, \tag{4}$$

the particular format of Eq. (1). Within definition (3), $\mathbb{C}'(s) = d\mathbb{C}(s)/ds$ denotes the total differential of the current stiffness operator (2) with respect to time s. For a complete discussion, especially the computation of $\dot{\Psi}$, the interested reader is referred to [1].

Remark The notation used for energy density functions has been modified compared to our previous contribution: traditional potentials—here equipped with temporally evolving parameters—are subsequently denoted by Φ while the true accumulated free energy density of a curing material is described by Ψ.

For the usually iterative solution of boundary value problems it is convenient to operate with a discrete update formula for constitutive equation (1), e.g. with

$$\boldsymbol{S}^{n+1} = \boldsymbol{S}^n + \frac{1}{2}\mathbb{C}^{n+1} : [\boldsymbol{C}^{n+1} - \boldsymbol{C}^n] \tag{5}$$

as resulting from implicit Euler backward integration. Numerical schemes like the Newton–Raphson method then additionally require a consistent linearisation of (5), the so-called *tangent operator* relating increments in strain to those in stress. For the present case one obtains

$$\mathbb{E}^{n+1} = 2\frac{\partial \boldsymbol{S}^{n+1}}{\partial \boldsymbol{C}^{n+1}} = \mathbb{C}^{n+1} + [\boldsymbol{C}^{n+1} - \boldsymbol{C}^n] : \mathfrak{A}^{n+1}, \tag{6}$$

whereas the sixth-order tensor $\mathfrak{A}^{n+1} = \partial\mathbb{C}^{n+1}/\partial\boldsymbol{C}^{n+1}$ describes changes of the cure dependent stiffness operator with respect to the current strain.

By utilising the above equations a *phenomenological* (Neo-Hooke) as well as a *micromechanical* (21-chain) viscoelasticity model will be extended towards the simulation of curing materials. Both approaches share an important assumption that is frequently used in modelling finite viscoelasticity, namely the additive decomposition of the free energy density into (elastic) equilibrium and (viscous) non-equilibrium parts:

$$\Phi = \Phi_{\text{eq}} + \Phi_{\text{neq}}. \tag{7}$$

The main difference between phenomenological and micromechanical viscoelasticity is twofold: While the latter utilises different formats for the two parts of the free energy density that are both dependent on the same list of strain-like quantities, the former usually assumes the same functional relation for Φ_{eq} and Φ_{neq}, but in terms of different variables which is motivated by kinematical considerations, mostly a multiplicative decomposition of the deformation gradient. The essential idea used here to extend standard viscoelasticity towards curing materials simply adapts energy decomposition (7) by setting

$$\Psi = \Psi_{\text{eq}} + \Psi_{\text{neq}}, \tag{8}$$

wherein the first part Ψ_{eq} is chosen according to definition (3), i.e. in terms of some standard equilibrium free energy $\Phi_{\text{eq}}(t)$ with evolving parameters and providing the current stiffness $\mathbb{C}_{\text{eq}}(t)$. To minimise complexity, Ψ_{neq} is simply identified with the corresponding non-equilibrium free energy density Φ_{neq}. This ansatz requires the concession that all stiffness-like parameters contained in Φ_{neq} are time-independent, i.e. only *inelasticity* parameters like the viscosity are chosen to evolve during curing in order to capture

the deceleration of relaxation processes. That this particular simplification does not imply an unphysical restriction becomes obvious in view of its consequences on the behaviour of the standard three-element model for viscoelastic solids (a Maxwell element in parallel to a spring). Fixing the stiffness of the spring, which is connected in series to the dashpot and, therefore, constitutes a parameter of Φ_{neq}, is not *qualitatively* modifying the overall stress response. While time proceeds, the dashpot opening completely relaxes the deformation of this spring, i.e. its contribution to the stress vanishes and only the spring in parallel to the Maxwell element is defining the material response by its time-dependent parameters. Thus it is sufficient to choose appropriate temporal evolutions for the parameters contained in Φ_{eq} to capture curing induced stiffness changes.

Energy decomposition (8) induces a corresponding decomposition of the stress response and, accordingly, of the tangent operator:

$$\boldsymbol{S} = \boldsymbol{S}_{\text{eq}} + \boldsymbol{S}_{\text{neq}}, \quad \mathbb{E} = \mathbb{E}_{\text{eq}} + \mathbb{E}_{\text{neq}}. \tag{9}$$

Decomposition $(9)_1$ can in turn be motivated by the just discussed classical rheological models, in particular the three-element standard solid containing a Maxwell element. In view of the above assumptions on Ψ_{eq} and Ψ_{neq}, equilibrium stress $\boldsymbol{S}_{\text{eq}}$ and tangent operator $\mathbb{E}_{\text{eq}}$ are updated according to Eqs. (5) and (6), respectively, whereas their non-equilibrium counterparts are determined from Φ_{neq} as in standard viscoelasticity. All further details required for an implementation in finite element codes will be derived in the subsequent Sects. 2 and 3 for both the viscoelastic Neo-Hooke and the 21-chain model.

One of the most important effects in polymer curing, i.e. the reduction of specific volume, the so-called *curing shrinkage*, and its influence on the material behaviour will then be discussed in Sect. 4. To this end, both the application of a pre-defined strain-like shrinkage function as well as a multiplicative decomposition of the deformation gradient are investigated. The final Sect. 5 presents some numerical examples demonstrating that the models proposed here are well suited to reproduce all phenomena considered relevant in isothermal polymer curing.

2 Phenomenological example: viscoelastic Neo-Hooke curing model

Following the above-mentioned practice in phenomenological viscoelasticity the same functional relation—in this case the compressible Neo-Hooke model—is chosen as the basis for both parts of energy decomposition (8). To set Ψ_{eq} and Ψ_{neq} to be dependent on different arguments originates from the widely accepted kinematical assumption that a superposition of reversible and irreversible processes can be captured by multiplicatively decomposing the deformation gradient:

$$\boldsymbol{F} = \boldsymbol{F}_e \cdot \boldsymbol{F}_v. \tag{10}$$

Here, $\boldsymbol{F}_e$ is denoting elastic deformations while $\boldsymbol{F}_v$ can be understood as an internal variable defining the current state of a local stress-free intermediate configuration representing a relaxation mechanism like e.g. in a standard Maxwell element. Materials exhibiting multiple relaxation mechanisms can be modelled analogously by extending (10) to a sum of the form $\boldsymbol{F} = \boldsymbol{F}_e^i \cdot \boldsymbol{F}_v^i$, cf. e.g. Lubliner [3] or Reese and Govindjee [4]. The decomposition of $\boldsymbol{F}$ provides two strain measures, i.e. the elastic and the viscous right Cauchy-Green tensor $\boldsymbol{C}_e$ and $\boldsymbol{C}_v$, respectively:

$$\boldsymbol{C}_e = \boldsymbol{F}_e^t \cdot \boldsymbol{F}_e = \boldsymbol{F}_v^{-t} \cdot \boldsymbol{C} \cdot \boldsymbol{F}_v^{-1}, \quad \boldsymbol{C}_v = \boldsymbol{F}_v^t \cdot \boldsymbol{F}_v, \tag{11}$$

the latter describing inelastic strains in the dashpot of the Maxwell element. The two parts of free energy density (8) are assumed to depend on these strain measures according to

$$\Psi = \Psi_{\text{eq}}(\boldsymbol{C}) + \Psi_{\text{neq}}\left(\boldsymbol{C}_e = \boldsymbol{F}_v^{-t} \cdot \boldsymbol{C} \cdot \boldsymbol{F}_v^{-1}\right). \tag{12}$$

The corresponding constitutive equations can be derived from the entropy inequality which, in case of the here assumed isothermal processes, reduces to the dissipation or Clausius–Duhem inequality

$$\boldsymbol{S} : \dot{\boldsymbol{C}} - 2\,\dot{\Psi} \geq 0, \tag{13}$$

where $(\dot{\bullet})$ again denotes the material time derivative. By calculating $\dot{\Psi}$ from (12) in consideration of Eq. (10) this can in turn be particularised to

$$\left[\boldsymbol{S} - 2\frac{\partial \Psi_{\text{eq}}}{\partial \boldsymbol{C}} - 2\boldsymbol{F}_v^{-1} \cdot \frac{\partial \Psi_{\text{neq}}}{\partial \boldsymbol{C}_e} \cdot \boldsymbol{F}_v^{-t}\right] : \frac{1}{2}\dot{\boldsymbol{C}} - \frac{\partial \Psi_{\text{neq}}}{\partial \boldsymbol{C}_e} : \frac{\partial \boldsymbol{C}_e}{\partial \boldsymbol{F}_v} : \dot{\boldsymbol{F}}_v \geq 0, \tag{14}$$

cf. e.g. [5] for a detailed derivation. From this, the standard argumentation due to Coleman and Gurtin [6] yields the conditional equations for the equilibrium and non-equilibrium stress in Eq. $(9)_1$ as

$$\boldsymbol{S} = 2\frac{\partial \Psi_{\text{eq}}}{\partial \boldsymbol{C}} + 2\boldsymbol{F}_v^{-1} \cdot \frac{\partial \Psi_{\text{neq}}}{\partial \boldsymbol{C}_e} \cdot \boldsymbol{F}_v^{-t} =: \boldsymbol{S}_{\text{eq}} + \boldsymbol{S}_{\text{neq}}. \tag{15}$$

The two parts of the stress response are now specified according to the aforementioned assumptions on the free energy density of curing materials, cf. Sect. 1. For the **equilibrium part** $\boldsymbol{S}_{\text{eq}}$ we insert the elastic Neo-Hookean curing model from [1], i.e. the accumulated equilibrium energy density $\Psi_{\text{eq}}(t)$ is given by Eq. (3), for which the current stiffness operator $\mathbb{C}_{\text{eq}}(t)$ has to be computed via (2) from

$$\Phi_{\text{eq}}(\boldsymbol{C}, J, t) = \frac{\kappa(t)}{2}\ln^2 J - \mu(t)\ln J + \frac{\mu(t)}{2}[I_1 - 3]. \tag{16}$$

This standard compressible Neo-Hookean energy density (16) is governed by the *cure dependent* elastic Lamé parameters $\kappa(t)$ and $\mu(t)$, the first invariant of the right Cauchy–Green tensor $I_1 = \boldsymbol{C} : \boldsymbol{I}$ and $J = \det \boldsymbol{F}$. In view of the consistency discussion sketched above, this particular choice of $\Psi_{\text{eq}} = \Psi_{\text{eq}}(\Phi_{\text{eq}})$ results in relation (1) for the equilibrium stress, the discrete update version of which reads

$$\boldsymbol{S}_{\text{eq}}^{n+1} = \boldsymbol{S}_{\text{eq}}^{n} + \frac{1}{2}\mathbb{C}_{\text{eq}}^{n+1} : \left[\boldsymbol{C}^{n+1} - \boldsymbol{C}^{n}\right]. \tag{17}$$

The particular forms of the current stiffness included as well as the additionally required tangent operator have previously [1] been derived as

$$\mathbb{C}_{\text{eq}}^{n+1} = \kappa^{n+1}\mathbb{A} - 2\left[\mu^{n+1} - \kappa^{n+1}\ln J\right]\mathbb{B} \tag{18}$$

$$\mathbb{E}_{\text{eq}}^{n+1} = \mathbb{C}_{\text{eq}}^{n+1} + \left[\boldsymbol{C}^{n+1} - \boldsymbol{C}^{n}\right] : \mathfrak{A}^{n+1} \quad \text{with} \tag{19}$$

$$\mathfrak{A}^{n+1} = \kappa^{n+1}\left[\mathfrak{B} + 2\ln J\,\mathfrak{C} + \mathbb{B}\otimes\boldsymbol{C}^{-1}\right] - 2\mu^{n+1}\mathfrak{C}, \tag{20}$$

cf. Eqs. (16, 17), and (20, 21) in [1] for the component-wise representations of the auxiliary quantities

$$\mathbb{A} = \boldsymbol{C}^{-1}\otimes\boldsymbol{C}^{-1}, \quad \mathfrak{B} = \partial\mathbb{A}/\partial\boldsymbol{C} \tag{21}$$

$$\mathbb{B} = \partial\boldsymbol{C}^{-1}/\partial\boldsymbol{C}, \quad \mathfrak{C} = \partial\mathbb{B}/\partial\boldsymbol{C}. \tag{22}$$

Concerning the **second part** $\boldsymbol{S}_{\text{neq}}$ of constitutive equation (15), i.e. the inelastic stress response, we identify $\Psi_{\text{neq}} = \Phi_{\text{neq}}$ and, once more, substitute the compressible Neo-Hookean ansatz (16) which, according to (12), is now dependent on the elastic right Cauchy–Green strain tensor:

$$\begin{aligned}\Psi_{\text{neq}} &= \Phi_{\text{neq}}\big(\boldsymbol{C}_e = \boldsymbol{F}_v^{-t}\cdot\boldsymbol{C}\cdot\boldsymbol{F}_v^{-1}, J_e\big)\\ &= \frac{\kappa_e}{2}\ln^2 J_e - \mu_e\ln J_e + \frac{\mu_e}{2}\left[I_{1e} - 3\right].\end{aligned} \tag{23}$$

Therein, $I_{1e} = \boldsymbol{C}_e : \boldsymbol{I}$, $J_e = \sqrt{\det\boldsymbol{C}_e}$ and the two additional Lamé parameters κ_e and μ_e are chosen to be *cure independent*, i.e. constant, as has been motivated in Sect. 1. The desired non-equilibrium stress follows again by evaluation of (15) from which one obtains

$$\begin{aligned}\boldsymbol{S}_{\text{neq}} &= 2\boldsymbol{F}_v^{-1}\cdot\frac{\partial\Phi_{\text{neq}}}{\partial\boldsymbol{C}_e}\cdot\boldsymbol{F}_v^{-t}\\ &= \boldsymbol{F}_v^{-1}\cdot\left[\kappa_e\ln J_e\boldsymbol{C}_e^{-1} + \mu_e\left[\boldsymbol{I} - \boldsymbol{C}_e^{-1}\right]\right]\cdot\boldsymbol{F}_v^{-t}\\ &= \kappa_e\ln J_e\,\boldsymbol{C}^{-1} + \mu_e\left[\boldsymbol{C}_v^{-1} - \boldsymbol{C}^{-1}\right]\end{aligned} \tag{24}$$

after recalling $\partial I_{1e}/\partial\boldsymbol{C}_e = \boldsymbol{I}$, $\partial J_e/\partial\boldsymbol{C}_e = \frac{1}{2}J_e\boldsymbol{C}_e^{-1}$ and exploiting Eq. (11). Note that the cure dependency of the inelastic material properties has not been considered yet but is implicitly present in the strain-like internal variable $\boldsymbol{C}_v$, whose current value needs to be determined now. To this end, exploiting the second part

$$-\frac{\partial\Psi_{\text{neq}}}{\partial\boldsymbol{C}_e} : \frac{\partial\boldsymbol{C}_e}{\partial\boldsymbol{F}_v} : \dot{\boldsymbol{F}}_v \geq 0 \tag{25}$$

of dissipation inequality (14) provides, after some rigorous mathematical manipulations the details of which can be found e.g. in [4], a non-linear evolution equation for $\boldsymbol{C}_v$. By assuming only small deviations from thermodynamical equilibrium, this equation can in turn be linearised, cf. e.g. [7], to obtain a rather simple ordinary differential equation which is frequently used in finite linear viscoelasticity [3,8–11]:

$$\dot{\boldsymbol{C}}_v = T^{-1}\left[\boldsymbol{C} - \boldsymbol{C}_v\right]. \tag{26}$$

It is important to note that the assumptions and simplifications leading to (26) imply some rather strong restrictions (strain rate close to zero, only small creep/relaxation) of the model in comparison to real viscoelastic material behaviour. Since this contribution mainly addresses curing phenomena, for which this most simple version of viscoelasticity is sufficiently instructive, further discussions on this subject are omitted here and we refer to the pertinent literature on finite viscoelasticity concerning more sophisticated and physically reasonable nonlinear evolution equations for internal variables.

One particular feature of (26), especially in view of computational costs, is its linearity since it obviates the application of iterative schemes for updating the internal variable $\boldsymbol{C}_v$, a procedure that is required at every Gauss point and time step. Furthermore, (26) is structurally identical to the standard evolution equation known from small strain linear viscoelasticity, compare also [2]. The additional material constant T arising in (26) denotes the relaxation time, a parameter that is time-dependent in case of curing materials:

$$\dot{\boldsymbol{C}}_v = T(t)^{-1}\left[\boldsymbol{C} - \boldsymbol{C}_v\right]. \tag{27}$$

Application of implicit Euler-backward integration then provides the rather simple discrete update equation for the internal variable $\boldsymbol{C}_v$:

$$\boldsymbol{C}_v^{n+1} = \underbrace{\frac{\Delta t}{T^{n+1} + \Delta t}}_{=:\,\omega^{n+1}}\boldsymbol{C}^{n+1} + \frac{T^{n+1}}{T^{n+1} + \Delta t}\boldsymbol{C}_v^{n}, \tag{28}$$

whereas T^{n+1} denotes the current relaxation time and $\Delta t = t_{n+1} - t_n$ is the current time step length. Inserting this into (24) concludes, together with (17) and (18), the constitutive relations for the viscoelastic Neo-Hookean curing model.

To obtain the remaining non-equilibrium part $\mathbb{E}_{\text{neq}}$ of tangent operator $(9)_2$, the derivative of the non-equilibrium stress $(24)_3$ with respect to the strain has to be computed.

From the chain rule and some tensor calculus we find

$$\begin{aligned}\mathbb{E}_{\text{neq}} &= 2\frac{\partial \boldsymbol{S}_{\text{neq}}}{\partial \boldsymbol{C}} \\ &= 2\kappa_e \ln J_e \frac{\partial \boldsymbol{C}^{-1}}{\partial \boldsymbol{C}} + 2\kappa_e \boldsymbol{C}^{-1} \otimes \frac{\partial \ln J_e}{\partial \boldsymbol{C}} \\ &\quad + 2\mu_e \left[\frac{\partial \boldsymbol{C}_v^{-1}}{\partial \boldsymbol{C}_v} : \frac{\partial \boldsymbol{C}_v}{\partial \boldsymbol{C}} - \frac{\partial \boldsymbol{C}^{-1}}{\partial \boldsymbol{C}} \right]. \end{aligned} \tag{29}$$

Therein, abbreviation $\mathbb{B}$ as given in Eq. $(22)_1$ may be used and $\partial \boldsymbol{C}_v / \partial \boldsymbol{C} = \omega \mathbb{I}^{sym}$ holds with $\mathbb{I}^{sym} = \frac{1}{2}[\delta_{ik}\delta_{jl} + \delta_{il}\delta_{jk}]$ since only the first term in Eq. (28) is dependent on the current strain. Furthermore, we define $\mathbb{D} := \partial \boldsymbol{C}_v^{-1} / \partial \boldsymbol{C}_v$, the component-wise representation of which is given by

$$(\mathbb{D})_{ijkl} = -\frac{1}{2}\left[(\boldsymbol{C}_v^{-1})_{ik}(\boldsymbol{C}_v^{-1})_{jl} + (\boldsymbol{C}_v^{-1})_{il}(\boldsymbol{C}_v^{-1})_{jk} \right]. \tag{30}$$

The multiplicative decomposition of the deformation gradient implies $J = J_e J_v$, i.e. $\ln J_e = \ln J - \ln J_v$. Using this, the derivative $\partial \ln J_e / \partial \boldsymbol{C}$ in (29) can, due to the chain rule and $\partial J_{(v)} / \partial \boldsymbol{C}_{(v)} = \frac{1}{2}\boldsymbol{C}_{(v)}^{-1}$, be simplified to

$$\frac{\partial \ln J_e}{\partial \boldsymbol{C}} = \frac{1}{J}\frac{\partial J}{\partial \boldsymbol{C}} - \frac{1}{J_v}\frac{\partial J_v}{\partial \boldsymbol{C}} = \frac{1}{2}\boldsymbol{C}^{-1} - \frac{\omega}{2}\boldsymbol{C}_v^{-1}. \tag{31}$$

Insertion of (31) into (29) finally yields the current non-equilibrium tangent operator

$$\begin{aligned}\mathbb{E}_{\text{neq}}^{n+1} &= \kappa_e \left[2 \ln J_e \, \mathbb{B} + \boldsymbol{C}^{-1} \otimes \left[\boldsymbol{C}^{-1} - \omega^{n+1} \boldsymbol{C}_v^{-1} \right] \right] \\ &\quad + 2\mu_e \left[\omega^{n+1} \mathbb{D} - \mathbb{B} \right], \end{aligned} \tag{32}$$

which concludes, together with Eqs. (22), (28), (30) and (19), the derivation of the tangent operator for the viscoelastic Neo-Hooke curing model. Note that double contractions with $\mathbb{I}^{sym}$ can be omitted since all strain measures are symmetric by definition.

3 Micromechanical example: viscoelastic 21-chain curing model

Similar to our previous contribution [1] on elastic curing models, we will in the following resort to the 21-chain micro-macro unit sphere model developed by Miehe and co-workers, now in its viscoelastic version published in [12]. Thereby, all parts of the model that describe chain interactions, which is done by considering the contraction of the cross section of a tube confining the polymer chain, are neglected for the sake of simplicity. Furthermore, we assume affine relationships between micro-kinematical quantities and their continuum counterparts for both the elastic and viscolastic networks, not only for the latter. The extension necessary to capture viscous curing behaviour is, once more, based on the time dependence of the viscous material parameters, e.g. the relaxation times.

The 21-chain viscoelastic curing model utilises the same assumptions on the decomposition of free energy density, stress response and tangent operator that are reflected by Eqs. (8) and (9). The **equilibrium part** Ψ_{eq} is defined according to (3) by inserting the current stiffness operator resulting from the compressible 21-chain energy density as given in [1], Eq. (26):

$$\Phi_{\text{eq}} = \sum_{i=1}^{21} \mu N w_i \left[\gamma_i \lambda_i^r + \ln \frac{\gamma_i}{\sinh \gamma_i} \right] + \frac{\kappa}{2} \ln^2 J - \mu \ln J. \tag{33}$$

This function represents a homogenisation of the behaviour of 21 Langevin chains that are oriented uniformly within a unit sphere and each consist of a cure dependent number $N = N(t)$ of Kuhn segments [13]. While the two latter terms describe the volumetric behaviour in terms of the usual, time dependent Lamé parameters, the sum is combining the chain contributions in terms of their orientation dependent relative stretches $\lambda_i^r = \sqrt{N^{-1}\boldsymbol{C} : [\boldsymbol{t}_i \otimes \boldsymbol{t}_i]}$ and a Padé approximation of the inverse Langevin function:

$$\gamma_i := \mathcal{L}^{-1}(\lambda_i^r) \approx \lambda_i^r [3 - (\lambda_i^r)^2][1 - (\lambda_i^r)^2]^{-1}. \tag{34}$$

The weights w_i and direction vectors $\boldsymbol{t}_i$ are given in the appendix of [1]. The corresponding current equilibrium stress $\boldsymbol{S}_{\text{eq}}^{n+1}$ is computed according to Eq. (17) whereas the current stiffness operator

$$\begin{aligned}\mathbb{C}_{\text{eq}}^{n+1} &= \sum_{i=1}^{21} w_i \frac{4\mu^{n+1} N^{n+1}}{\left[N^{n+1} - \lambda_i^2 \right]^2} \left[\boldsymbol{t}_i \otimes \boldsymbol{t}_i \otimes \boldsymbol{t}_i \otimes \boldsymbol{t}_i \right] \\ &\quad + \kappa^{n+1} \mathbb{A} - 2\left[\mu^{n+1} - \kappa^{n+1} \ln J \right] \mathbb{B} \end{aligned} \tag{35}$$

has to be inserted, cf. also Eq. (27) in [1]. The current equilibrium tangent operator $\mathbb{E}_{\text{eq}}^{n+1}$ again follows relation (19) and additionally requires

$$\begin{aligned}\mathfrak{A}^{n+1} &= \sum_{i=1}^{21} w_i \frac{8\mu^{n+1} N^{n+1}}{\left[N^{n+1} - \lambda_i^2 \right]^3} \left[\boldsymbol{t}_i \otimes \boldsymbol{t}_i \otimes \boldsymbol{t}_i \otimes \boldsymbol{t}_i \otimes \boldsymbol{t}_i \otimes \boldsymbol{t}_i \right] \\ &\quad + \kappa^{n+1} \left[\mathfrak{B} + 2 \ln J \, \mathfrak{C} + \mathbb{B} \otimes \boldsymbol{C}^{-1} \right] - 2\mu^{n+1} \mathfrak{C} \end{aligned} \tag{36}$$

with the chain stretch $\lambda_i = \sqrt{N}\lambda_i^r$ and abbreviations $\mathbb{A}$, $\mathbb{B}$, $\mathfrak{B}$, $\mathfrak{C}$ as used in the previous section. Concerning the temporal evolution of the relevant material parameters and especially their interdependencies the interested reader is referred to Sect. 5 in [1].

The **non-equilibrium part** realises inelastic behaviour by superimposing a network of viscoelastic chains that are connected via entanglements to the elastic network, which itself has been the basis for Eq. (33). These chains are not only

deformed with the elastic network but additionally able to relax their stretch state by untangling their loose ends, which in turn increases the number of active Kuhn segments, cf. [12,14] for a schematic visualisation. This dynamic process is modelled phenomenologically by extending the elastic free energy density φ_i of a single chain oriented along $\boldsymbol{t}_i$ (compare Eq. (24) in [1]) with

$$\varphi_i^v = \frac{\mu_v}{2}\left[\ln\lambda_i - \varepsilon_i\right]^2, \quad i = 1,\dots,21, \tag{37}$$

as proposed by Miehe and Göktepe [12]. The tube constraint part has again been neglected and μ_v, ε_i denote a cure independent, phenomenological material parameter and a strain-like internal variable governing the non-equilibrium stress of the chain, respectively. Relation (37) can easily be extended towards multiple relaxation mechanisms if reformulated as a sum, similar to the addition of further Maxwell elements in the phenomenological case. We omit this possibility for simplicity and restrict all following considerations to only one relaxation mechanism.

The corresponding continuum non-equilibrium free energy Φ_{neq}, which defines $\Psi_{\text{neq}} = \Phi_{\text{neq}}$ as before, is now obtained from the same procedure of homogenising chain contributions over the unit sphere that already led to (33), i.e.

$$\Phi_{\text{neq}} = \langle\varphi_i^v\rangle = \frac{1}{2}\sum_{i=1}^{21} w_i\,\mu_v\left[\ln\lambda_i - \varepsilon_i\right]^2, \tag{38}$$

where the ε_i successively relax the initial elastic chain stretches $\lambda_i = \sqrt{\boldsymbol{C} : [\boldsymbol{t}_i \otimes \boldsymbol{t}_i]}$. Energetically conjugated micro forces driving the evolution of the strain-like ε_i can, according to Miehe and Göktepe [12], be defined by

$$\beta_i := -\frac{\partial\varphi_i^v}{\partial\varepsilon_i} = \mu_v\left[\ln\lambda_i - \varepsilon_i\right]. \tag{39}$$

By assuming appropriate functions to describe the dissipation at the chain level and after some calculations the details of which can be found in [12] or [15], the constraint of non-negative micro dissipation provides the following non-linear evolution equation for β_i:

$$\dot{\beta}_i + \frac{\beta_i}{T}\left|\beta_i\right|^{\delta-1} - \frac{\mu_v}{\lambda_i}\dot{\lambda}_i = 0 \quad \text{with } \beta_i(t=0) = 0. \tag{40}$$

Therein, $\delta > 0$ denotes a constant material parameter while $|\bullet|$ is the absolute value relieved of units. To describe curing materials, the relaxation time T in (40) is again set to be cure dependent, i.e. $T = T(t)$, and assumed to evolve according to an exponential saturation function as proposed for our small-strain curing model, cf. Eq. (38) in [2]:

$$T(t) = T_0 + [T_\infty - T_0]\left[1 - \exp(-\kappa_\tau t)\right]. \tag{41}$$

Here, T_0, T_∞ are initial and final relaxation time, respectively, and κ_τ describes the reduction rate of the viscosity during curing, i.e. the decrease of the untangling velocity of the chains. Evolution equation (40) has to be solved iteratively at every Gauss point for every time step and chain orientation $\boldsymbol{t}_i$, e.g. by Newton's method, for which a detailed recipe is given in Table 1. Regarding memory requirements it is worth noting that all chain forces β_i and stretches λ_i from the previous load step have to be stored. The current non-equilibrium stress tensor then reads

$$\boldsymbol{S}_{\text{neq}}^{n+1} = 2\frac{\partial\Phi_{\text{neq}}}{\partial\boldsymbol{C}} = \sum_{i=1}^{21} w_i\,\frac{\beta_i^{n+1}}{\lambda_i}\,[\boldsymbol{t}_i \otimes \boldsymbol{t}_i] \tag{42}$$

and the current non-equilibrium tangent operator follows accordingly as twice the derivative of the stress with respect to the strain, i.e.

$$\mathbb{E}_{\text{neq}}^{n+1} = \sum_{i=1}^{21} w_i\left[\frac{c_i^{n+1}}{\lambda_i^2} - \frac{\beta_i^{n+1}}{\lambda_i^3}\right][\boldsymbol{t}_i \otimes \boldsymbol{t}_i \otimes \boldsymbol{t}_i \otimes \boldsymbol{t}_i], \tag{43}$$

cf. again to [12,15] for detailed derivations. For the sake of clarity, only terms containing cure dependent quantities are indicated by superscript $n+1$ in both equations.

Table 1 Update procedure for the non-equilibrium micro-forces β_i

(i) Given from previous time step t_n are stretch and strain for all chain orientations $\boldsymbol{t}_i$, i.e. $\left\{\left(\lambda_i^n, \beta_i^n\right) \mid i = 1,\dots,21\right\}$.

(ii) Compute current chain stretches $\lambda_i^{n+1} = \sqrt{\boldsymbol{C}^{n+1} : [\boldsymbol{t}_i \otimes \boldsymbol{t}_i]}$ with current deformation gradient: $\boldsymbol{C}^{n+1} = \boldsymbol{F}^t(t_{n+1}) \cdot \boldsymbol{F}(t_{n+1})$.

(iii) Determine β_i^{n+1} by applying Newton's method to the Euler backward solution of Eq. (40), i.e. the non-linear equation

$$\beta_i^{n+1}\left[1 + \frac{\Delta t}{T^{n+1}}\left|\beta_i^{n+1}\right|^{\delta-1}\right] - \beta_i^n + \mu_v\left[\frac{\lambda_i^n}{\lambda_i^{n+1}} - 1\right] =: r_i(\beta_i^{n+1}) \overset{!}{=} 0$$

is solved by iteratively updating β_i^{n+1} according to

$${}^k\beta_i^{n+1} = {}^{k-1}\beta_i^{n+1} - \frac{r_i({}^{k-1}\beta_i^{n+1})}{r_i'({}^{k-1}\beta_i^{n+1})}, \quad k = 1,\dots, \quad {}^0\beta_i^{n+1} := \beta_i^n,$$

until $r_i({}^k\beta_i^{n+1}) < tol$ and where

$$r_i'({}^k\beta_i^{n+1}) = \left[1 + \frac{\Delta t}{T^{n+1}}\left|{}^k\beta_i^{n+1}\right|^{\delta-1}\right] + \frac{\Delta t}{T^{n+1}}[\delta - 1]\left|{}^k\beta_i^{n+1}\right|^{\delta-3}\left[\beta_i^{n+1}\right]^2.$$

(iv) Compute the current chain tangent moduli $c_i := d\beta_i/d\lambda_i$ from

$$c_i^{n+1} = \frac{\mu_v}{\left[\lambda_i^{n+1}\right]^2 r_i'(\beta_i^{n+1})} - \frac{\beta_i^{n+1}}{\lambda_i^{n+1}}.$$

(v) Insert the current β_i^{n+1}, c_i^{n+1} into the stress tensor and tangent operator, i.e. Eqs. (42) and (43), respectively.

4 Modelling curing shrinkage

One of the prominent phenomena in polymer curing is the *shrinkage effect*, i.e. the reduction of the specific volume due to chain growth and/or cross linking. In case of specimen held within fixed boundaries during curing, this can

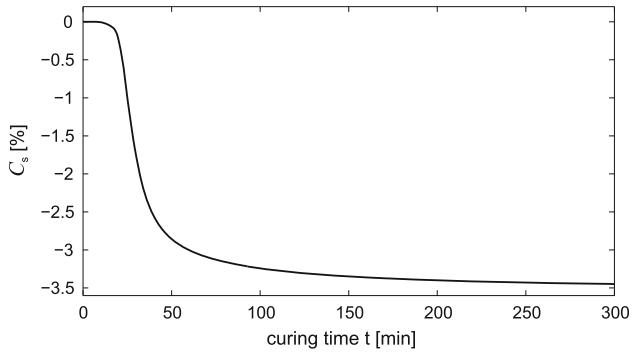

Fig. 1 Evolution of shrinkage function (44) in case of $[p_1, p_2, p_3, p_4, p_5, p_6] = [-1.129, 37.36 \text{ min}, 1.261, -2.402, -25.74 \text{ min}, 4.611]$

lead to significant residual stresses and/or strains, where the former may even surpass the plastic yield strength. The relevance of this effect is dependent on the time of gelation, before which the material can hardly develop any stresses, as well as on the inelastic characteristics afterwards which may allow relaxation of the shrinkage stresses. Especially in case of epoxies with high relaxation times but essentially elasto-plastic behaviour, the influences of the curing shrinkage may even impede certain applications like structural bonding in automotive frame and body construction due to unacceptable sheet deformation.

Two phenomenological approaches to incorporate the shrinkage effect into constitutive models have been proposed in the literature so far: (1) the superposition of an exponentially decaying shrinkage strain function, which has been introduced by Kiasat [16], and (2) a multiplicative decomposition of the deformation gradient, advocated by Lion and Höfer [17]. In the following subsections, both ansatzes will be incorporated to the above proposed methods for curing simulations.

4.1 Shrinkage strain function

This rather basic, nonetheless successful approach to consider volume shrinkage utilises a prescribed, cure/time dependent volumetric strain function which is simply superimposed to the current deformation state during the simulation. Kiasat [16], for example, proposed the following, exponentially decaying scalar function

$$C_s(t) = p_1 \exp\left(-\left[\frac{p_2}{t}\right]^{p_3}\right) + p_4 \exp\left(-\left[\frac{p_5}{t}\right]^{p_6}\right), \tag{44}$$

which is governed by six parameters p_i that have to be determined experimentally. A specification of this function, which is also used in the forthcoming examples, is plotted in Fig. 1.

The incorporation of this in the form of a volumetric strain to the above proposed curing models is realised by modifying update equation (17) for the current equilibrium stress according to

$$\boldsymbol{S}_{\text{eq}}^{n+1} = \boldsymbol{S}_{\text{eq}}^{n} + \frac{1}{2}\mathbb{C}_{\text{eq}}^{n+1} : [[\boldsymbol{C}^{n+1} - C_s^{n+1}\boldsymbol{I}] - [\boldsymbol{C}^{n} - C_s^{n}\boldsymbol{I}]], \tag{45}$$

i.e. a correction of both the previous and current strain state is introduced. Since C_s is independent of $\boldsymbol{C}$, the linearisation of (45) with respect to the right Cauchy–Green strain provides the correspondingly modified current equilibrium tangent operator:

$$\mathbb{E}_{\text{eq}}^{n+1} = \mathbb{C}_{\text{eq}}^{n+1} + [[\boldsymbol{C}^{n+1} - C_s^{n+1}\boldsymbol{I}] - [\boldsymbol{C}^{n} - C_s^{n}\boldsymbol{I}]] : \mathfrak{A}^{n+1}. \tag{46}$$

To clarify the procedure, the incorporation of volume shrinkage has been restrained to the equilibrium material response. A consideration of shrinkage within the non-equilibrium part is straight-forward and will be illustrated by an example in Sect. 5 to demonstrate the relaxation of shrinkage stresses in viscoelastic materials.

It is worth noting that the phenomenological consideration of curing shrinkage as done in Eq. (45) has not yet been proven to be thermodynamically consistent. The superposition of a volumetric strain increases the amount of energy stored in the specimen—although there is no external work applied in a mechanical sense. The gain in strain energy due to shrinkage is, in fact, here assumed to be balanced with the release of chemical energy during chain and network formation, similar to temperature increases in case of exothermal reactions. Both thermal and chemical energy parts are not considered here but will be incorporated and discussed in a future contribution.

4.2 Multiplicative decomposition

The application of a multiplicative decomposition of the deformation gradient within the context of curing and shrinkage has first been advocated by Lion and Höfer [17]. We will here omit the originally included thermal part and restrict ourselves to decomposing the deformation gradient into two parts, i.e. a stress producing mechanical part and a volume reducing shrinkage part:

$$\boldsymbol{F} = \boldsymbol{F}_m \cdot \boldsymbol{F}_s \quad \text{with } \boldsymbol{F}_s := [1 + \alpha s]^{1/3}\boldsymbol{I}. \tag{47}$$

Therein, $\alpha \in [0, 1]$ denotes the degree of cure, cf. [2], and $s \leq 0$ is a time dependent parameter controlling the magnitude of the shrinkage. Note that this ansatz can be (and is frequently) used to model e.g. growth phenomena in biomechanics [18]. Similar to phenomenological viscoelasticity, the following decomposition of the right Cauchy-Green tensor is implied by (47):

$$\boldsymbol{C} = \boldsymbol{F}^t \cdot \boldsymbol{F} = \boldsymbol{F}_s^t \cdot \boldsymbol{F}_m^t \cdot \boldsymbol{F}_m \cdot \boldsymbol{F}_s =: \boldsymbol{F}_s^t \cdot \boldsymbol{C}_m \cdot \boldsymbol{F}_s \tag{48}$$

which provides the conditional equation for the mechanical right Cauchy–Green strain as

$$\boldsymbol{C}_m = \boldsymbol{F}_m^t \cdot \boldsymbol{F}_m = \boldsymbol{F}_s^{-t} \cdot \boldsymbol{C} \cdot \boldsymbol{F}_s^{-1} = [1+\alpha s]^{-2/3}\boldsymbol{C}. \quad (49)$$

From the ususal thermodynamical argumentation that has already been used in the case of phenomenological viscoelasticity, the corresponding Piola–Kirchhoff stress is obtained to read

$$\boldsymbol{S} = \boldsymbol{F}_s^{-1} \cdot 2\frac{\partial \Psi_m}{\partial \boldsymbol{C}_m} \cdot \boldsymbol{F}_s^{-t} = [1+\alpha s]^{-2/3}\boldsymbol{S}_m, \quad (50)$$

with the cure dependent mechanical free energy density Ψ_m. Thus, the total stress resulting from mechanical load and superimposed curing shrinkage is equal to the purely mechanical stress $\boldsymbol{S}_m$, as computed e.g. from Eq. (15) with (17) and (24), pre-multiplied by $\boldsymbol{F}_s^{-2}$. More generally, this can be understood as a pull-back operation from the stress-free intermediate configuration to the reference configuration. The corresponding chemical potential providing the strain energy which is required by the shrink as well as the thermodynamical consistency have been discussed in [17].

The necessary tangent operator is again obtained from linearising the stress with respect to the strain for which the chain rule yields

$$\begin{aligned}\mathbb{E} &= 2\frac{\partial \boldsymbol{S}}{\partial \boldsymbol{C}} = 2\frac{\partial \boldsymbol{S}}{\partial \boldsymbol{C}_m} : \frac{\partial \boldsymbol{C}_m}{\partial \boldsymbol{C}} \\ &= 2\frac{\partial \left([1+\alpha s]^{-2/3}\boldsymbol{S}_m\right)}{\partial \boldsymbol{C}_m} : \frac{\partial \left(\boldsymbol{F}_s^{-t} \cdot \boldsymbol{C} \cdot \boldsymbol{F}_s^{-1}\right)}{\partial \boldsymbol{C}} \\ &= [1+\alpha s]^{-4/3}\mathbb{E}_m, \end{aligned} \quad (51)$$

with $\mathbb{E}_m = 2\partial \boldsymbol{S}_m/\partial \boldsymbol{C}_m$ denoting the mechanical tangent operator that has to be calculated e.g. from Eq. (19) or (32).

5 Numerical examples

Several numerical examples are presented in this section to demonstrate that the proposed models are suitable to reproduce the mechanical behaviour of viscoelastic polymers during isothermal curing, which is, in particular, characterised by a stiffness gain, decelerating relaxation effects and a volumetric shrinkage. All simulations have been performed using a research-based in-house finite element code that has been extended by the constitutive relations and tangent operators summarised in the previous sections. First, some one-dimensional examples reflect the behaviour of a single eight-noded brick element under prescribed uniaxial stretch histories and parameter evolutions. Next, several three-dimensional simulations are presented to demonstrate both inhomogeneous deformation behaviour and the effects induced by the curing shrinkage.

Due to the lack of sufficient experimental data on the temporal evolution of material parameters we resort to arbitrary but reasonable choices. Concerning the equilibrium shear modulus μ the previously used [1] exponential saturation function, whose format is also assumed for the relaxation time, cf. Eq. (41), is applied:

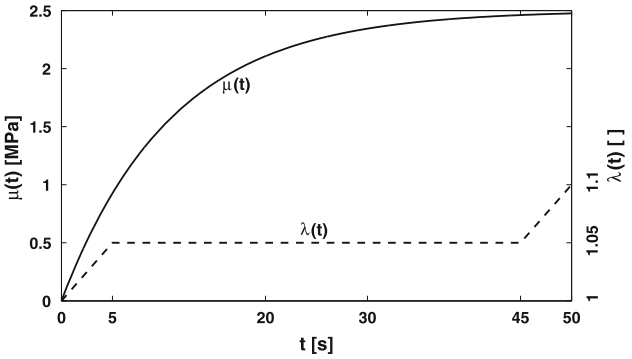

Fig. 2 Three phase load history $\lambda(t)$ and exemplary evolution of the shear modulus $\mu(t)$ with $[\mu_0, \mu_\infty, \kappa_\mu] = [0.0001\ \text{MPa}, 2.5\ \text{MPa}, 0.0925\,\text{s}^{-1}]$

$$\mu(t) = \mu_0 + [\mu_\infty - \mu_0]\left[1 - \exp(-\kappa_\mu t)\right]. \quad (52)$$

It is governed by the initial and final shear modulus μ_0 and μ_∞, respectively, as well as the curvature parameter κ_μ. A specification of (52) is plotted in Fig. 2. For the sake of simplicity, the elastic bulk modulus is calculated via $\kappa(t) = \frac{2}{3}\mu(t)[1+\nu][1-\nu]^{-1}$ from the prescribed shear modulus evolution, whereas a constant Poisson's ratio of $\nu = 0.35$ has been assumed. For the 21-chain model, an initial number N_0 of chain segments is prescribed and the resulting temporal evolution $N(t)$ follows from that of the shear modulus, cf. the discussion on conservation of mass in [1]. The non-equilibrium parameters κ_e, μ_e, μ_v are kept at constant values, only the relaxation time evolves according to (41).

5.1 Homogeneous one-dimensional examples

First, simple uniaxial tension tests are simulated using a single finite element to check whether the proposed curing models will correctly reproduce the gain in stiffness, the behaviour in case of the strain rate being zero and the deceleration of relaxation processes during the advancement of curing. Concerning the first two properties we consider a three phase deformation history that consists of (1) a linear increase to a (macroscopic) stretch $\lambda = 1.05$ within the first 5 s, followed by (2) a 40 s holding phase and (3) another linear increase to $\lambda = 1.1$ during the last 5 s, cf. Fig. 2. This load history is applied to both the compressible Neo-Hooke and 21-chain viscoelastic curing model, whereas only the elastic parameters are evolving but the relaxation time is kept fixed for the moment. Fig. 3 depicts the resulting stress responses versus time and stretch, the parameters used are given in the caption. Both models obviously behave

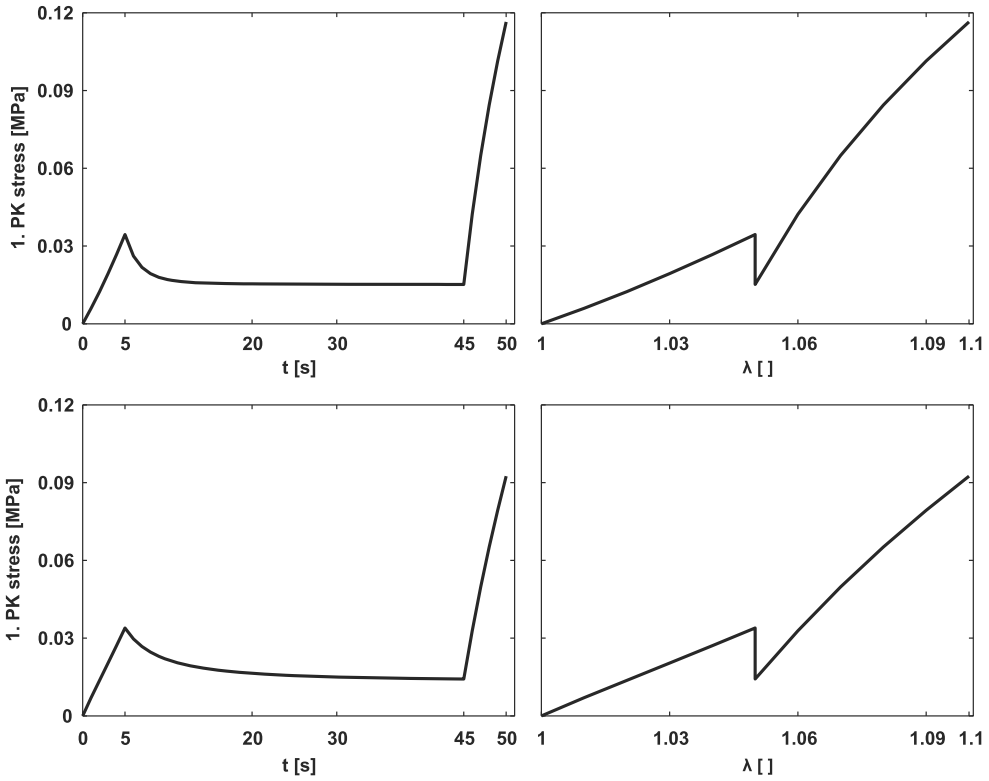

Fig. 3 Response of a curing viscoelastic material with constant relaxation time under the stretch history of Fig. 2. Piola stress versus time (*left*) and stretch (*right*), each for the Neo-Hooke model (*top*) with $[\mu_0, \mu_\infty, \kappa_\mu, \kappa_e, \mu_e, T, \Delta t] = [0.001\ \text{MPa}, 0.5\ \text{MPa}, 0.0925\,\text{s}^{-1}, 10.5\ \text{MPa}, 0.75\ \text{MPa}, 3\ \text{s}, 1\ \text{s}]$ and the 21-chain model (*bottom*) with $[\mu_0, \mu_\infty, \kappa_\mu, N_0, \mu_v, T, \delta, \Delta t] = [0.001\ \text{MPa}, 0.5\ \text{MPa}, 0.0925\,\text{s}^{-1}, 5 \times 10^4, 5.5\ \text{MPa}, 1.2\ \text{s}, 1.5, 1\ \text{s}]$

viscoelastic, as is indicated by the decrease in stress during the holding phase. The ongoing increase in stiffness has no impact on the stress in case of a constant deformation state, which is reflected by the horizontal lines in the left-hand figures after the relaxation has reached its equilibrium. Within the right-hand side figures, the stiffness gain is clearly observable by comparing the slopes of the curves before and after the holding phase at $\lambda = 1.05$. The different magnitudes of the stress increase during the two loading phases (left-hand side figures) do also reflect this.

To demonstrate the effects that arise if also the viscoelastic properties are evolving, the above stretch history is modified to three linear loading phases of 2 s duration which are interleaved with two holding phases each lasting for 20 s. The responses are plotted in Fig. 4 and clearly indicate the desired deceleration of viscous relaxation processes for both models since the equilibrium stresses are reached much later within the second holding phases. Furthermore, slower relaxation time evolutions are also correctly captured as can be observed from the higher stress peaks at the end of each loading phase.

5.2 Inhomogeneous three-dimensional example

Concerning viscoelastic curing behaviour in three dimensions we consider a plate with a hole in its center to realise inhomogeneous stress distributions under load. Its dimensions are $60 \times 12 \times 2\,\text{mm}^3$ and the hole has a diameter of 6 mm. The plate is discretised by 544 eight-noded hexagonal elements and supported as depicted in Fig. 5 (most left). A uniaxial extension in x-direction is applied within 22 s, which is followed by 168 s of relaxation. These two steps are repeated a second time to check the evolution of elastic and viscous material properties. Fig. 5 (left) depicts both the deformation and the resulting Cauchy stresses in x-direction, the latter obviously are decreasing during the holding phases. The right-hand side compares the behaviour of two nodes which are chosen such that their stress levels after the first and second loading phase are equal. The curves clearly indicate the desired deceleration of relaxation processes (curves between the dashed lines) as well as the gain in stiffness (different magnitudes of stress growth during the loading phases) and the constant stress in cases where the strain rate becomes zero (after the relaxation has reached equilibrium).

5.3 Curing shrinkage simulations

5.3.1 Shrinkage strain function

Concerning the shrinkage induced stress build-up during cure, a three-dimensional block of $20 \times 7 \times 3\,\text{mm}^3$, discretised

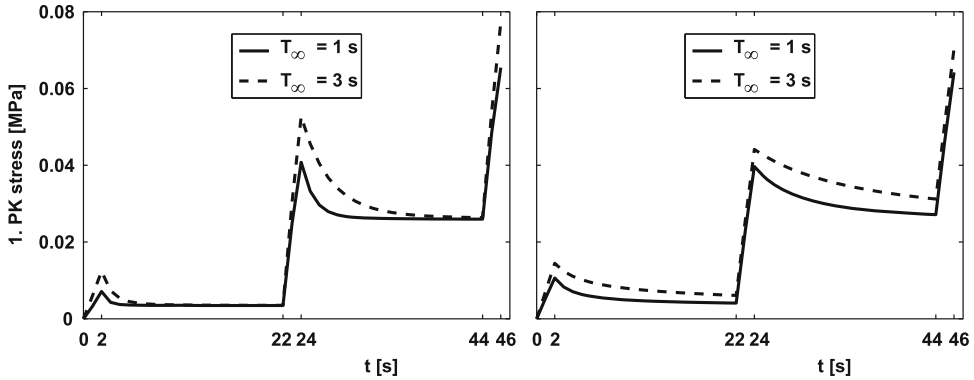

Fig. 4 Curing viscoelastic material subjected to a five phase stretch history. Piola stress versus time for two different final relaxation times T_∞. *Left* Neo-Hooke with $[\mu_0, \mu_\infty, \kappa_\mu, \kappa_e, \mu_e, T_0, T_\infty, \kappa_\tau, \Delta t] = [0.001\ \text{MPa}, 0.5\ \text{MPa}, 0.0925\,\text{s}^{-1}, 10.5\ \text{MPa}, 0.75\ \text{MPa}, 0.015\ \text{s}, \mathbf{1\ vs.\ 3\ s}, 0.0925\,\text{s}^{-1}, 1\,\text{s}]$. *Right* 21-chain with $[\mu_0, \mu_\infty, \kappa_\mu, N_0, \mu_v, T_0, T_\infty, \kappa_\tau, \delta, \Delta t] = [0.001\ \text{MPa}, 0.5\ \text{MPa}, 0.0925\ \text{s}^{-1}, 5 \times 10^4, 5.5\ \text{MPa}, 0.015\ \text{s}, \mathbf{1\ vs.\ 3\ s}, 0.0925\ \text{s}^{-1}, 1.5, 1\ \text{s}]$

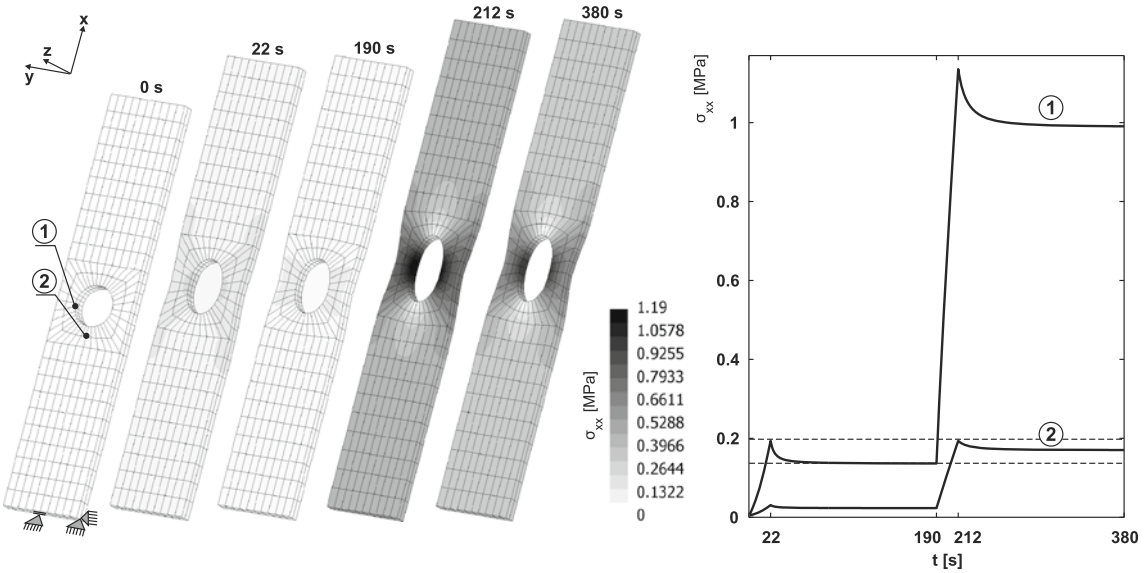

Fig. 5 Three-dimensional boundary value problem: plate with centered hole, subjected to a four phase stretch history (pull, hold, pull, hold) and modelled by the viscoelastic 21-chain curing model with $[\mu_0, \mu_\infty, \kappa_\mu, N_0, \mu_v, T_0, T_\infty, \kappa_\tau, \delta, \Delta t] = [0.0001\ \text{MPa}, 2.0\ \text{MPa}, 0.0115\ \text{s}^{-1}, 2 \times 10^6, 10.5\ \text{MPa}, 0.015\ \text{s}, 4.2\ \text{s}, 0.0115\ \text{s}^{-1}, 1.5, 1\ \text{s}]$. *Left* Cauchy stress and deformation at relevant time steps. *Right* Comparison of stress versus time for two nodes having the same stress level at the beginning of the first and second relaxation phase, respectively. The deceleration of relaxation processes is clearly visible from the fact that node ② relaxes much slower to a higher equilibrium stress after $t = 212$ s than node ① does between $t = 22...190$ s. The gain in stiffness is again reflected by the much higher stress increase during the second loading phase

by one hundred eight-noded brick elements, is considered. Its front and back side are kept fixed while all longitudinal sides are free to deform. The curing shrinkage is modelled by the shrinkage strain function approach described in Sect. 4.1, which is here applied to the elastic Neo-Hooke curing model. Figure 6 depicts deformation and Cauchy-stresses after 270 min of curing under the assumption of Kiasat's [16] volume shrinkage function as given in Fig. 1. Both the resulting deformations and stresses do obviously attain magnitudes that should be considered carefully in design and dimensioning of structures.

5.3.2 Multiplicative decomposition

To illustrate shrinkage simulations relying on the multiplicative decomposition of the deformation gradient we adapt a setup for a thin three-dimensional plate that has been used by Retka and Höfer [19]. The plate has an extension of $40 \times 10 \times 0.5\ \text{mm}^3$ and is discretised by 800 linear brick elements. Three different bearing conditions are assumed, cf. Fig. 7, as well as a final volume reduction of ten percent, i.e. $s = -0.1$ in Eq. $(47)_2$. The degree of cure α is simply assumed to evolve according to an exponential

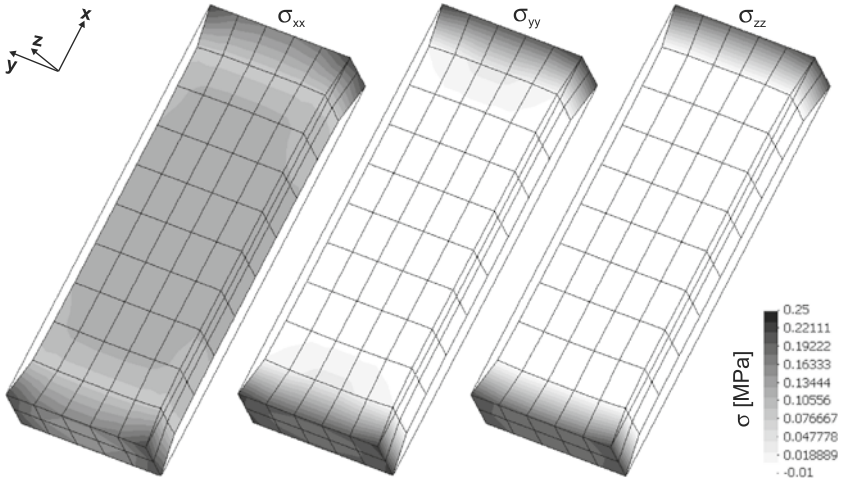

Fig. 6 Block without external load but fixed transverse ends. Deformation (scaled by two) and Cauchy stresses due to shrinkage after 270 min of curing. Elastic Neo-Hooke curing model with $[\mu_0, \mu_\infty, \kappa_\mu] = [0.0001$ MPa, 1.5 MPa, 0.02 $s^{-1}]$, extended by the shrinkage strain function approach of Sect. 4.1

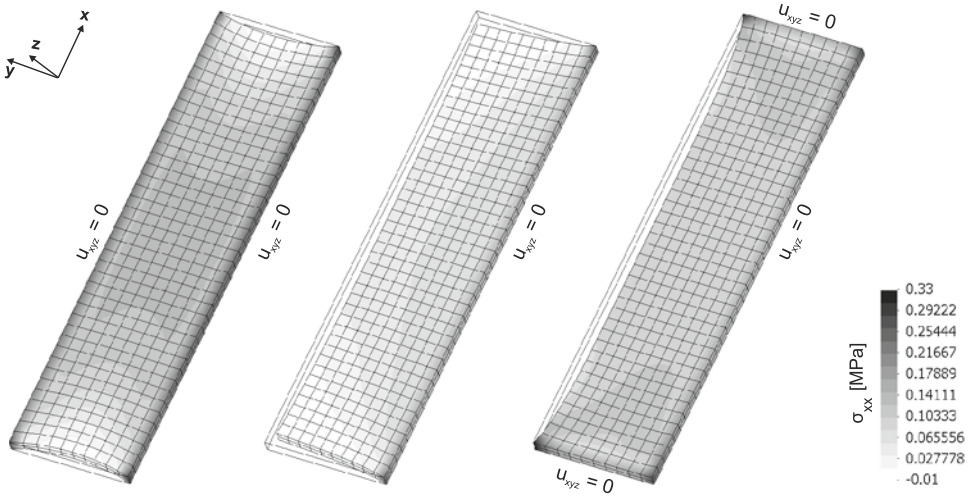

Fig. 7 Curing shrinkage of a thin three-dimensional plate subjected to three different bearing conditions, deformation (scaled by two) and Cauchy stress in x-direction after 20 s of curing. Elastic 21-chain curing model, extended by the multiplicative decomposition approach of Sect. 4.2. Model parameters: $[\mu_0, \mu_\infty, \kappa_\mu, N_0] = [0.0001$ MPa, 1.5 MPa, 0.25 s^{-1}, $2 \times 10^6]$

saturation function like (52), which has already been used for shear modulus and relaxation time, whereas now $[\alpha_0, \alpha_\infty, \kappa_\alpha] = [0.0001, 1.0, 0.25\ s^{-1}]$. More sophisticated approaches for the evolution of α, as mentioned e.g. in [2], are not considered here for the sake of simplicity but are, nonetheless, straightforwardly to incorporate. Note that the initial degree of cure—as well as the initial shear modulus—has to have a small positive value for numerical reasons. Figure 7 depicts the bearing specific deformations as well as the Cauchy stresses in x-direction after 20 s of curing, simulated with the elastic 21-chain curing model together with the shrinkage model equations of Sect. 4.2.

5.3.3 Curing shrinkage and viscoelasticity

The shrinkage phenomenon is of particular interest for viscoelastic materials that are able to decrease the arising stresses via relaxation already during curing—which would be the case for a majority of polymer materials. To demonstrate the behaviour for the case of these reverse processes being simultaneously active we resort to the block example from Sect. 5.3.1 and compare elastic and viscoelastic simulations. By applying the viscoelastic 21-chain curing model with multiplicative decomposition shrinkage, 'elastic' behaviour is mimicked by choosing a constant and, in view of the curing process duration, infinite relaxation time while real 'viscoelastic' behaviour allowing for significant relaxation already during curing is realised with parameters similar to those from Fig. 5. The decrease of shrinkage induced residual stresses can be of remarkable magnitude, as is indicated by both the contour plots and the dispersing stress curves in Fig. 8.

6 Conclusion and outlook

Extending the previous part of this contribution, phenomenological and micro-mechanically based material models for the finite strain simulation of viscoelastic polymers that undergo curing processes and volume shrinkage have been proposed. The governing constitutive equations and the tangent operators are derived and the numerical realisation

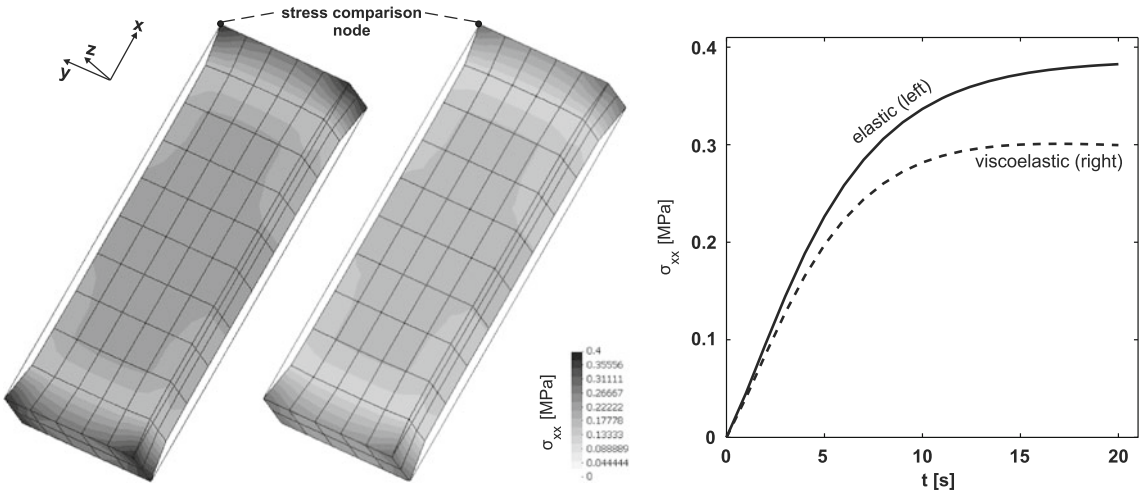

Fig. 8 Stress development in a block held at fixed length during curing, simulated with the viscoelastic 21-chain curing model together with the multiplicative decomposition approach for the volume shrinkage. Deformation (scaled by two) and Cauchy stress in x-direction after 20 s of curing for, (*left*) the 'elastic' case with long ($T = 1500$ s) and constant relaxation time and, (*middle*) the viscoelastic case with short and evolving relaxation time ($[T_0, T_\infty, \kappa_\tau] = [0.015\text{ s}, 4.2\text{ s}, 0.25\text{ s}^{-1}]$) time. Remaining model parameters: $[\mu_0, \mu_\infty, \kappa_\mu, N_0, \mu_v, \delta, \Delta t] = [0.0001\text{ MPa}, 2.0\text{ MPa}, 0.25\text{ s}^{-1}, 2 \times 10^6, 10.5\text{ MPa}, 1.5, 1\text{ s}]$. Comparison of stress over time for the top left node (*right*)

within the finite element framework is sketched. The numerical examples demonstrate that the developed models are suitable to correctly reproduce the relevant phenomena. Further extensions considering effects like exothermal reactions, thermoelastic coupling and elastoplastic material behaviour will be subject of forthcoming research.

It is worth noting that the presented simulation results are somewhat academic so far since both the underlying material parameters as well as their evolutions were chosen arbitrarily and are not related to a specific material. The deformation ranges considered here are, furthermore, too small to reveal the quantitative and qualitative differences between simple phenomenological polymer models and the more sophisticated micromechanical chain models. Merely the computational costs as well as the application or a specific material under consideration may be useful to decide in favour of a particular approach. The most important issue in curing simulations is still posed by the experimental determination of the necessary evolutions experienced by the mechanical material parameters.

Acknowledgments Financial support by the German Research Foundation (DFG) within the collaborative project PAK 108 is gratefully acknowledged.

References

1. Hossain M, Possart G, Steinmann P (2009) A finite strain framework for the simulation of polymer curing. Part I. Elasticity. Comput Mech 44(5):621–630
2. Hossain M, Possart G, Steinmann P (2009) A small-strain model to simulate the curing of thermosets. Comput Mech 43(6):769–779
3. Lubliner J (1985) A model of rubber viscoelasticity. Mech Res Commun 12(2):93–99
4. Reese S, Govindjee S (1998) A theory of finite viscoelasticity and numerical aspects. Int J Solids Struct 35:3455–3482
5. Kleuter B (2007) Generalized parameter identification for finite viscoelasticity. PhD Thesis, University of Kaiserslautern, Germany
6. Coleman BD, Gurtin ME (1967) Thermodynamics with internal state variables. J Chem Phys 47:597–613
7. Govindjee S, Reese S (1997) A presentation and comparison of two large deformation viscoelasticity models. J Eng Mater Technol 119:251–255
8. Reese S (2003) A micromechanically motivated material model for the thermo-viscoelastic material behaviour of rubber-like materials. Int J Plasticity 19:909–940
9. Johlitz M, Steeb H, Diebels S, Chatzouridou A, Batal J, Possart W (2007) Experimental and theoretical investigation of nonlinear viscoelastic polyurethane systems. J Mater Sci 42:9894–9904
10. Huber N, Tsakmakis C (2000) Finite deformation viscoelasticity laws. Mech Mater 32:1–18
11. Amin AFMS, Lion A, Sekita S, Okui Y (2006) Nonlinear dependence of viscosity in modeling the rate-dependent response of natural and high damping rubbers in compression and shear: Experimental identification and numerical verification. Int J Plasticity 22:1610–1667
12. Miehe C, Göktepe S (2005) A micro–macro approach to rubber-like materials. Part-II. The micro-sphere model of finite rubber viscoelasticity. J Mech Phys Solids 53:2231–2258
13. Kuhn W, Grün F (1942) Beziehungen zwischen elastischen Konstanten und Dehnungsdoppelbrechung hochelastischer Stoffe. Kolloid-Zeitschrift 101:248–271
14. Bergström JS, Boyce MC (1998) Constitutive model of the large-strain time-dependent behaviour of elastomers. J Mech Phys solids 46:931–954
15. Göktepe S (2007) Micro–macro approaches to rubbery and glassy polymers: predictive micromechanically-based models and simulations. PhD Thesis, University of Stuttgart, Germany
16. Kiasat M (200) Curing shrinkage and residual stresses in viscoelastic thermosetting resins and composites. PhD Thesis, TU Delft, Netherlands

17. Lion A, Höfer P (2007) On the phenomenological representation of curing phenomena in continuum mechanics. Arch Mech 59: 59–89
18. Himpel G (2008) Computational modeling of biomechanical phenomena—remodeling, growth and reorientation. PhD Thesis, University of Kaiserslautern, Germany
19. Retka J, Höfer P (2007) Numerische Simulation aushärtender Klebstoffe. Diploma Thesis, Universität der Bundeswehr München